```
@inproceedings{gill2023applicability,
  author = {Hyunjune Gill and Seongkyu Lee and Marius L. Ruh and John T. Hwang},
  title = {Applicability of Low-Fidelity Tonal and Broadband Noise Models on Small-Scale
    Rotors},
  booktitle = {AIAA SciTech 2023 Forum},
  year = {2023}
}
```

Applicability of Low-Fidelity Tonal and Broadband Noise Models on Small-Scale Rotors

Hyunjune Gill* and Seongkyu Lee†
Department of Mechanical and Aerospace Engineering
University of California, 1 Shields Avenue, Davis, CA 95616, USA

Marius L. Ruh‡ and John T. Hwang§
Department of Mechanical and Aerospace Engineering
University of California, 9500 Gilman Dr, La Jolla, CA 92093, USA

This paper presents the application of steady and unsteady frequency-domain propeller tonal noise and empirical helicopter broadband noise models for drone or small-scale rotor noise. These models provide a quick assessment of rotor noise, which is useful during the initial stages of aircraft design or optimization. Four frequency-domain tonal noise prediction models and three empirical broadband noise models are validated and compared using small rotor cases to analyze the predictive capabilities and limitations of these models. It is found that the steady frequency-domain models tend to over-predict the tonal noise at the fundamental blade passing frequency, and these models cannot capture noise along the rotor axis, thus resulting in a significant under-prediction near the rotor axis. This limitation is overcome by the unsteady frequency-domain model, but this model is limited to hover flight only. Moreover, the empirical broadband noise models show large over-predictions on a small rotor with a relatively higher thrust coefficient. Since these broadband noise models are not found to be robust, a more accurate model is needed to be developed for small rotor applications.

Nomenclature

A_b	=	total blade area, m^2
A_x	=	airfoil cross-sectional area, approximated as $0.6853bh$, m^2
B	=	number of blades
b	=	blade chord, m
$C_{l\alpha}$	=	lift slope
C_P	=	power coefficient
C_T	=	thrust coefficient
c	=	speed of sound, m/s
c_{mB}	=	acoustic pressure due to loading, Pa
D	=	rotor diameter, m
F	=	Prandtl's tip loss factor
$H_\nu^{(1)}$	=	Hankel function of the first kind
$H_\nu^{(2)}$	=	Hankel function of the second kind
h	=	maximum airfoil thickness, m
Δh	=	wake spacing parameter
J_ν	=	bessel function of the first kind
k	=	reduced frequency
k_x	=	wave number
M	=	freestream Mach number

*Ph.D Student, AIAA Student Member; hjgill@ucdavis.edu
†Associate Professor, AIAA Associate Fellow; skulee@ucdavis.edu
‡Ph.D Student, AIAA Student Member; mruh@ucsd.edu
§Assistant Professor, AIAA Senior Member; jhwang@eng.ucsd.edu

MCA	=	mid-chord alignment, m
M_b	=	blade sectional Mach number, $\Omega r/c$
M_s	=	section relative Mach number, $\sqrt{M^2 + r^2 M_t^2}$
M_t	=	tip Mach number
m	=	acoustic harmonic number
P_{mL}, P_{mT}	=	root mean square acoustic pressure due to loading and thickness, Pa
R	=	radial distance of a rotor from the center to the blade tip, m
r	=	normalized radial distance, R/r_t
r_t	=	rotor tip radius, D/2, m
S	=	observer distance from rotor hub, $\sqrt{x^2 + y^2 + z^2}$, m
S_0	=	amplitude radius, $\sqrt{x^2 + (1 - M^2)Y^2}$, m
S_r	=	S in retarded time frame, m
SPL_{150}	=	sound pressure level at 150 m away from the rotor hub along the rotor axis, dB
SPL_{tonal}	=	tonal sound pressure level, dB
s_0	=	distance between rotor hub and observer, m
v_i	=	induced velocity, m/s
x, y, z	=	observer location coordinates relative to rotor hub, m
Y	=	observer distance from rotor axis, $\sqrt{y^2 + z^2}$, m
λ	=	load harmonic number
λ_i	=	inflow ratio
Ω	=	angular velocity, rad/s
Ψ_L, Ψ_V	=	normalized loading and thickness source transforms
ϕ	=	tangential angle in Hanson model, $\arctan(z/y)$, rad
ϕ	=	induced angle of attack in Kvurt and Stalnov model, rad
ϕ_s	=	phase lag due to sweep, rad
ϕ_t	=	blade angle relative to rotor plane, rad
ϕ'	=	ϕ relative to rotor axis, rad
ρ	=	air density, kg/m^3
σ	=	rotor solidity
θ	=	observer angle relative to flight direction, $\arccos(x/S)$, rad
θ_0	=	elevation angle relative to the rotor plane, rad
θ_r	=	θ in retarded time frame, rad
θ'_r	=	θ_r relative to rotor axis, rad
$\theta(r)$	=	blade pitch angle distribution, rad

Introduction

Blade noise is one of the most significant noise sources for rotorcraft, which can be divided into tonal and broadband noise. Tonal noise, also known as rotational noise, is low-frequency sound produced by periodic sound pressure disturbances as a blade rotates around its shaft axis; broadband noise, which is also referred to as vortex noise in the literature, is high-frequency sound generated by random fluctuations of the forces on the blade due to turbulence [1]. Tonal noise is composed of thickness and loading noise [2], while broadband noise is composed of many other sources, such as turbulence ingestion noise, blade wake interaction noise, airfoil self-noise including turbulent boundary layer (TBL) trailing-edge noise, laminar boundary layer (LBL) vortex shedding noise, bluntness noise, stall noise, and tip vortex formation noise. TBL trailing-edge noise is often the most dominant noise source [3, 4] in airfoil self-noise. There are numerous models and solutions, ranging from empirical to physics-based models and analytical solutions, that have been developed to predict these tonal and broadband noise sources.

Tonal noise can be predicted using either a time-domain or a frequency-domain method. A time-domain method originated from the Ffowcs Williams-Hawkings (FW-H) equation, which was developed as the extension of the Lighthill-Curle theory of aerodynamic sound for an arbitrarily moving surface [2]. Farassat [5] developed Formulation 1A, which is an integral solution of the FW-H equation, to analytically describe the thickness and loading noise. This method collects a time history of the pressure perturbations on the surface to predict tonal noise with great accuracy, but it requires the computation of retarded time and the time-dependent sectional aerodynamic loading to obtain accurate noise predictions. Recently, high-fidelity computational fluid dynamics (CFD) coupled with the FW-H equation has been used to predict urban air mobility (UAM) aircraft noise [6–8]. With high-fidelity simulations, the tonal and broadband noise predictions can be accurately obtained for various rotor sizes and flight conditions; however, high-fidelity models are costly. In the rapidly growing UAM or drone industry, it is necessary to have tools that can quickly produce noise predictions with sufficient accuracy, especially for vehicle optimization that involves hundreds or thousands of noise computations. Frequency-domain methods, on the other hand, eliminate the computation of retarded time by taking the Fourier transform of the wave equation, thus requiring less computational cost than the time-domain method. Thus, the frequency-domain methods are suitable for multidisciplinary optimization due to fast computations. Gutin [9] first developed an analytical acoustic theory for steady propeller noise in frequency domain in 1936 by assuming a ring of dipole noise sources at an effective radius, which was later modified by Deming [10] in 1937 to include the noise generated from the finite blade thickness. Since then, many advanced acoustic theories in the frequency domain have been developed; a formulation by Barry and Magliozzi [11] is capable of predicting tonal noise for axial forward flight by including the doppler effect, and a formulation by Hanson [12, 13] considers non-compactness and includes the effect of blade sweep in addition to an axial forward flight noise prediction capability.

Rotor broadband noise predictions are more difficult than tonal noise predictions since broadband noise is stochastic noise composed of multiple noise sources [14–16]. There is no analytical expression that can describe broadband noise, but many physics-based models have been developed to predict individual components of broadband noise. Amiet [17] applied Schwarzschild's solution that was first introduced in electromagnetism for the scattering of a wave by the edge of a semi-infinite plate to develop trailing-edge noise theory. Roger and Moreau [18, 19] modified this theory to include leading-edge back scattering and to correct a pressure jump assumption at the trailing edge. Li and Lee [20] further modified this theory to apply the correction made by Roger and Moreau to only the scattered part of the pressure disturbance, not the incident part. This method has been shown effective in predicting broadband noise of a small-scale rotor [20], but it requires the computation of the wall pressure spectrum near the trailing edge [21, 22], which involves additional boundary-layer flow computations. The empirical models, on the contrary, only use rotor performance parameters as inputs to predict OASPL of broadband noise but not individual components of broadband noise. The first relevant understanding of the relationship between sound pressure level (SPL) and the rotor performance parameters was discovered by Yudin [23] by introducing an acoustic dipole model. Continued acoustic experiments by Davidson and Hargest [24] and Schlegel et al. [25] revealed that the blade tip velocity is scaled to the sixth power and the blade lift coefficient to the second power, while Stuckey and Goddard [26] scaled the lift coefficient to the power of 1.66. There have also been attempts to predict broadband noise spectrum. Pegg [27] tabulated changes in the sound pressure level from the peak value at multiple frequencies in one-third octave band to predict the broadband noise spectrum in a high frequency region.

The tonal noise prediction models that are studied in this paper have been validated against propellers by Herniczek et al. [28], which are similar to the UAM rotors in size. However, in the prior publication, not enough studies were performed to understand whether the existing tonal noise prediction models are capable of predicting noise from small-scale rotors, such as those of drones which are significantly smaller than the UAM rotors and have different blade pitch rates from those of propellers. Also, the broadband noise prediction tools studied in this paper are mainly developed from experiments with helicopter rotors. The primary goal of this paper is to investigate whether the existing frequency-domain tonal noise and empirical broadband noise prediction models are capable of predicting noise from small-scale rotors. The validity and limitations of these models are studied, which could yield room for improvement or could present an opportunity to develop a new model for tonal or broadband noise of small-scale rotors.

Methods

A total of seven low-fidelity rotor noise prediction models are explored in the present paper. Four of the noise models are frequency-domain tonal noise prediction models developed by Gutin and Deming [9, 10], Barry and Magliozzi [11], Hanson [12, 13], and Kvurt and Stalnov [29], respectively. The first three models use steady aerodynamic models. Herniczek et al. [28] summarized the advantages and disadvantages of each model for propeller noise predictions. The fourth tonal noise model uses an unsteady aerodyanmic model that improves noise predictions above and below the rotor plane. The coordinate system of a rotor used in these tonal noise prediction models is shown in Fig. 1. The rest of the noise models are empirical broadband noise prediction models developed by Davidson and Hargest [24], Schlegel, King, and Mull [25], and Stuckey and Goddard [26], respectively. These broadband noise models were empirically constructed from experiments with helicopters, such as CH-3C, CH53A, Wessex, HU-1A, and HU-1B. Johnson [1] collected these models and re-formulated them at a reference distance of 150 m below the rotor in terms of rotor

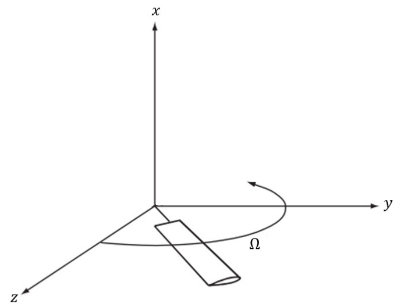

Fig. 1 Coordinate system used for the tonal noise prediction models.

performance parameters.

Blade Element Momentum Theory (BEMT)

The aerodynamic forces must first be computed to predict tonal and broadband noise. The classical Blade Element Momentum Theory (BEMT) is used to compute the steady sectional thrust and torque along the blade span. Blade Element Theory (BET) discretizes the rotor blade and analyzes aerodynamic forces section by section using local velocities and flow angles, while Momentum Theory (MT) computes momentum flux through the rotor annulus to compute the sectional thrust and power. These two theories are combined by equating the thrust equations to obtain a sectional inflow ratio along the blade span. The inflow ratio equation with Prandtl's tip loss factor (F) is shown below:

$$\lambda_i(r) = \frac{\sigma C_{l\alpha}}{16F}\left(\sqrt{1 + \frac{32F}{\sigma C_{l\alpha}}\theta(r)r} - 1\right) \tag{1}$$

where σ is rotor solidity, $C_{l\alpha}$ is the lift slope, and $\theta(r)$ is spanwise pitch distribution.

Once the inflow ratio along the blade span is computed, the sectional thrust and induced power can be computed using the following relationships:

$$\begin{aligned} dC_T &= 4F\lambda_i^2 r dr \\ dC_P &= \lambda_i dC_T \end{aligned} \tag{2}$$

Since C_P is equal to C_Q, the sectional torque (dQ/dr) that is necessary to predict tonal noise in the presented models can be obtained from the sectional power coefficient equation in Eq. (2). It is important to note that the sectional power does not include profile power. Since the noise is generated by the pressure reaction on the fluid, only the induced power is considered to compute the sectional torque distribution [1].

Tonal Noise

Gutin and Deming (GD)

Equations (3) and (4) give expressions for the acoustic pressure due to loading and thickness of rotor blades, respectively. These equations were developed and modified by Gutin [9] and Deming [10]. They used an effective radius instead of integrating the sectional thrust and torque, but Herniczek et al. [28] used the integral form over the blade span. These equations serve as a baseline of the two other formulations that are studied in the present paper. It should be noted that these formulations by Gutin and Deming are only suitable for a hovering rotor. The blade sectional thrust, $\frac{dT}{dR}$, and sectional torque, $\frac{dQ}{dR}$, are the main inputs from the aerodynamic tool, which was discussed in the previous section.

$$P_{mL} = \frac{mB\Omega}{2\pi\sqrt{2}cS}\int_{hub}^{tip}\left[\frac{dT}{dR}\cos\theta - \frac{dQ}{dR}\frac{c}{\Omega R^2}\right]J_{mB}\left(\frac{mB\Omega}{c}R\sin\theta\right)dR \tag{3}$$

$$P_{mT} = \frac{-\rho(mB\Omega)^2 B}{3\pi\sqrt{2}S}\int_{hub}^{tip} bhJ_{mB}\left(\frac{mB\Omega}{c}R\sin\theta\right)dR \tag{4}$$

Barry and Magliozzi (BM)

Barry and Magloizzi [11] further modified the equations for the acoustic pressure due to loading and thickness by including a doppler effect to incorporate an axial forward flight condition. The alternate Bessel functions, J_{mB+1} and J_{mB-1}, are used for a more exact far-field noise prediction. Two corrections were included by Herniczek et al. [28, 30] when deriving Eqs. (5) and (6): a sign correction was made in the Bessel function terms from both equations [31] and the power of 4 in the doppler effect term, $(1-M^2)^4$ from the original loading formulation [11], was removed to avoid a large over-prediction at higher forward Mach numbers [11].

$$P_{mL} = \frac{1}{\pi\sqrt{2}S_0}\int_{hub}^{tip}\frac{R}{b\cos\phi_t}\sin\left(\frac{mBb\cos\phi_t}{2R}\right)\left[\frac{(M+X/S_0)\Omega}{c(1-M^2)}\frac{dT}{dR}-\frac{1}{R^2}\frac{dQ}{dR}\right]\left[J_{mB}+\frac{(1-M^2)YR}{2S_0^2}(J_{mB-1}-J_{mB+1})\right]dR \quad (5)$$

$$P_{mT} = -\frac{\rho m^2\Omega^2 B^3}{2\pi\sqrt{2}(1-M^2)^2}\frac{(S_0+MX)^2}{S_0^3}\int_{hub}^{tip}A_x\left[J_{mB}+\frac{(1-M^2)YR}{2S_0^2}(J_{mB-1}-J_{mB+1})\right]dR \quad (6)$$

where

$$J_{mB} = J_{mB}\left(\frac{mB\Omega YR}{cS_0}\right) \quad (7)$$

Hanson (H)

Hanson's formulation [12] further extends the frequency-domain tonal noise prediction model to include non-compactness, sweep effect, and non-axial flow. Unlike the two previous formulations, Hanson's formulation is written in retarded time frame, variables of which are denoted by the subscript r.

$$P_{mL} = \frac{imBM_t\sin\theta_r\exp\left[imB(\frac{\Omega S_r}{c}+(\phi'-\frac{\pi}{2}))\right]}{2\pi\sqrt{2}Yr_t(1-M\cos\theta_r)}\int_{hub}^{tip}\left[\frac{\cos\theta_r'}{1-M\cos\theta_r}\frac{dT}{dr}-\frac{1}{r^2M_tr_t}\frac{dQ}{dr}\right]\exp(i\phi_s)J_{mB}\Psi_L\,dr \quad (8)$$

$$P_{mT} = \frac{-\rho c^2B\sin\theta_r\exp\left[imB(\frac{\Omega S_r}{c}+(\phi'-\frac{\pi}{2}))\right]}{4\pi\sqrt{2}(Y/D)(1-M\cos\theta_r)}\int_{hub}^{tip}M_s^2(h/b)\exp(i\phi_s)J_{mB}k_x^2\Psi_V\,dr \quad (9)$$

where

$$J_{mB} = J_{mB}\left(\frac{mBrM_t\sin\theta_r'}{1-M\cos\theta_r}\right) \quad (10)$$

The effect of chord-wise non-compactness is represented by the non-dimensional source transforms, Ψ_L and Ψ_V:

$$\Psi_L(k_x) = \begin{cases} 1 & \text{if } k_x = 0, \\ \frac{2}{k_x}\sin\frac{k_x}{2} & \text{if } k_x \neq 0. \end{cases} \quad (11)$$

$$\Psi_V(k_x) = \begin{cases} 2/3 & \text{if } k_x = 0, \\ \frac{8}{k_x^2}\left[\frac{2}{k_x}\sin\left(\frac{k_x}{2}\right)-\cos\left(\frac{k_x}{2}\right)\right] & \text{if } k_x \neq 0. \end{cases} \quad (12)$$

where k_x is a wave number defined as:

$$k_x = \frac{2mBbM_t}{M_s(1-M\cos\theta_r)} \quad (13)$$

The sweep effect is included in the phase lag represented by ϕ_s:

$$\phi_s = \frac{2mBM_t}{M_s(1-M\cos\theta_r)}\frac{MCA}{D} \quad (14)$$

The non-axial flow effect is included in the retarded time frame observer angle, θ_r', and tangential angle with respect to the propeller shaft axis, ϕ':

$$\cos\theta_r' = \cos\theta_r\cos\alpha + \sin\theta_r\sin\phi\sin\alpha \quad (15)$$

$$\cos\phi' = \frac{\sin\theta_r}{\sin\theta_r'}\cos\phi \quad (16)$$

where α is the pitch angle of propeller shaft axis relative to the flight direction.

Kvurt and Stalnov (KS)

The previous models assume steady aerodynamic loads during hover; however, in reality, unsteady loads may exist even during hover flight due to blade vibration, which could significantly contribute to the noise along the rotating axis. This model, presented by Kvurt and Stalnov [29], extends the Gutin model by including unsteadiness in the aerodynamic loads on a rotor. Unsteady loads are modeled by either Sears, $S(k)$, or Loewy, $C'(k, mB, h)$, function as follows:

$$S(k) = \frac{2}{\pi k}\left[H_0^{(1)}(k) + iH_1^{(1)}\right]^{-1} \tag{17}$$

$$C'(k, mB, \Delta h) = \frac{H_1^{(2)}(k) + 2J_1(k)W(k, mB, \Delta h)}{H_1^{(2)}(k) + iH_0^{(2)} + 2[J_1(k) + iJ_0(k)]W(k, mB, \Delta h)} \tag{18}$$

where Δh is a wake spacing parameter and $W(k, mB, \Delta h)$ is a vorticity weighting factor defined as follows:

$$\Delta h = \frac{4\pi v_i}{bB\Omega} \tag{19}$$

$$W(k, mB, \Delta h) = \frac{1 + e^{k\Delta hB} e^{i2\pi mB} \sum_{q=1}^{B-1} e^{-k\Delta hq}}{e^{kB\Delta h} e^{i2\pi mB} - 1} \tag{20}$$

Sears function models unsteady loads by a thin airfoil encountering a sinus gust, while Loewy function includes the correction due to a returning vorticity from its own blade's shed wake in a rotating system on top of the unsteady blade motion. The details of these functions can be found in references [29, 32]. Once either of these functions is determined, modeling of the unsteady loads using the steady loads from BEMT is completed with the following expression:

$$L_\lambda = A(k)L_{QS} + L_{NC} \tag{21}$$

$$T_\lambda^{'} = L_\lambda \cos\phi \tag{22}$$

$$D_\lambda^{'} = L_\lambda \sin\phi \tag{23}$$

where $A(k)$ is either Sears or Loewy function, L_{QS} is quasi-static lift obtained from BEMT, L_{NC} is non-circularly lift, and $T_\lambda^{'}$ and $D_\lambda^{'}$ are sectional thrust and drag for the corresponding load harmonics, respectively. The magnitude of the unsteady fluctuation is modeled by assuming 5% of the induced velocity per blade loading harmonic. The non-circularly lift is neglected since the unsteady fluctuation in the gust is not considered.

The unsteady loads are then substituted into the far-field noise formulation in Eq. (24) to predict loading noise for unsteady hover flight. It is noteworthy that unlike the previous models that use the sectional torque, this model uses the sectional drag. The detailed derivation of the model with unsteady loads can be found in reference [29].

$$c_{mB} = \frac{mB\Omega}{4\pi Sc}\int_{R_h}^{R_t}\left[\sum_{\lambda=0}^{\infty} i^{-(mB-\lambda B)} \times \left[T_\lambda^{'}\cos\theta - D_\lambda^{'}\frac{(mB-\lambda B)}{mBM_b}\right] J_{mB-\lambda B}(mBM_b\sin\theta)\right] dr \tag{24}$$

It is important to note that Kvurt and Stalnov only provided the loading component of the acoustic pressure for hover since the noise prediction along the rotor axis is of interest and the thickness noise along the rotor axis is expected to be negligible. At any other observer locations, an appropriate model for computing a thickness component of the acoustic pressure can be used to predict total tonal noise.

Before converting the pressure into decibel, the root mean square pressure must be determined first using the following expression:

$$P_{mL}^2 = \frac{c_{mB} \cdot c_{mB}^*}{2} \tag{25}$$

Once the acoustic pressure due to loading and thickness is computed from the presented models, the total tonal noise is predicted in decibels by using the following relationship:

$$SPL_{tonal} = 10\log_{10}\left(\frac{P_{mL}^2 + P_{mT}^2}{P_{ref}^2}\right) \tag{26}$$

where $P_{ref} = 2 \times 10^{-5}$.

Broadband Noise

Three empirical broadband noise models that are presented in the current study were collected and reformulated by Johnson [1] in terms of commonly shared variables: blade loading (C_T/σ) and blade tip speed (ΩR). The formulation by Davidson and Hargest [24] is derived from the Whirlwind and Dragonfly flight tests in addition to the Wessex rotor test. Schlegel et al. [25] derived their formulation from experiments with CH-3C and CH-53A rotors, and Stuckey and Goddard [26] derived their formulation based on whirl tower tests with a Wessex rotor. The resulting formulations after unit conversion from English unit to SI unit are provided in Eqs. (27), (28), and (29). Note that SPL in these equations indicates overall sound pressure level (OASPL), and the subscript 150 indicates OASPL measured at 150 m directly below the rotor.

Davidson and Hargest (DH)

$$SPL_{150} = 10\log_{10}\left[(\Omega R)^6 A_b (C_T/\sigma)^2\right] - 36.7 \tag{27}$$

Schlegel, King, and Mull (SKM)

$$SPL_{150} = 10\log_{10}\left[(\Omega R)^6 A_b (C_T/\sigma)^2\right] - 42.9 \tag{28}$$

Stuckey and Goddard (SG)

$$SPL_{150} = 10\log_{10}\left[(\Omega R)^6 A_b (C_T/\sigma)^{1.66}\right] - 39.9 \tag{29}$$

OASPL at an arbitrary observer location can be predicted using the following relationship [1]:

$$SPL = SPL_{150} + 20\log_{10}\left(\frac{\sin\theta_0}{s_0/150}\right) \tag{30}$$

It is important to note that θ_0 is an elevation angle from the rotor plane, while the observer angle used in the tonal noise models was measured from the propeller shaft axis (rotational axis).

Numerical Results

Verifications

The implemented frequency-domain tonal noise prediction models are first verified against a few selected cases from the list of test cases that Herniczek et al. [28, 30] and Kvurt and Stalnov [29] used. The steady aerodynamic forces on the rotor and its performance parameters are computed from BEMT, and the unsteady aerodynamic forces are obtained using the BEMT outputs and either Sears or Loewy function as shown in Eqs. (17) and (18), respectively. The performance outputs from BEMT are compared with the available experimental data to ensure the aerodynamic inputs to the noise models are accurate. However, there may still be some discrepancy in the thrust and torque distributions along the blade span since the distributions of the forces are not readily available in experiments to compare with the BEMT predictions, and the detailed polar data of the airfoils along the blade span are not available as well. The observer angles are measured from the propeller shaft axis; hence a 0-degree angle indicates the propeller shaft axis while a 90-degree angle indicates the propeller plane.

Table 1 shows the number of blades and radius of the rotors along with rotor operating conditions that are used to verify the steady frequency-domain models – Gutin-Deming (GD), Barry-Magliozzi (BM), and Hanson (H) models – and the unsteady frequency-domain model – Kvurt and Stalnov (KS). The steady models are compared against the measurement data and the predictions made by Herniczek et al. in Fig 2. Although the same frequency-domain formulations are used to predict the tonal noise, there are discrepancies between the current predictions and Herniczek et al.'s predictions due to uncertainties in the aerodynamic inputs. Despite the differences, the steady models – Gutin-Deming (GD), Barry-Magliozzi (BM), and Hanson (H) – show good predictions especially at observer angles between 30 and 60 degrees. All three models over-predict tonal noise near the rotor plane. Note that the discrepancy between the measurement data and the noise predictions is the largest at 0 degree observer angle. Since these frequency-domain tonal noise prediction models assume steady loading, the noise is expected to have a zero magnitude along the rotor

Table 1 **Geometries and flight conditions for the steady and unsteady model verifications.**

Model	Rotors	Blade Number	Radius (m)	Freestream Mach	RPM
Steady	W60LK18 [33]	2	0.6095	0.0	2150
	SR-3 [34]	2	0.324	0.2	7622
Unsteady	Mejzlik Heavy Duty [29]	3	0.3556	0.0	1500

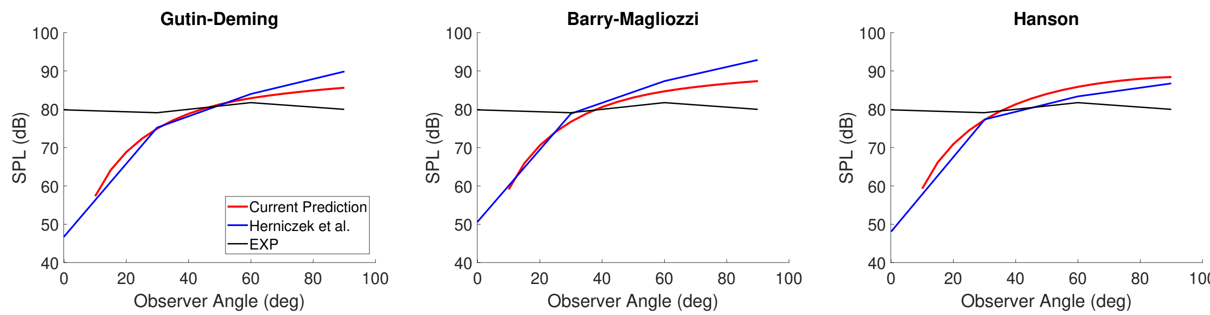

(a) (b) (c)

Fig. 2 Comparison of the first BPF tonal noise predictions of the W60LK18 rotor with the experimental data [33] measured at 3.6576 m (12 feet) away from the propeller hub and predictions made by Herniczek et al. [28, 30]: (a) Gutin-Deming, (b) Barry-Magliozzi, and (c) Hanson.

rotating axis; however, the experiments capture noise from unsteady loading as well, thus resulting in the higher noise levels at 0 degree observer angle.

The Kvurt-Stalnov (KS) model improves this limitation by including unsteady aerodynamic loads. Although this model is limited to hover flight only, it expands the capability of the frequency-domain model to predict noise along the rotating axis. The KS model is verified using the Mejzlik Heavy Duty rotor shown in Table 1. The details of the geometry, such as the spanwise chord distribution, blade thickness, and pitch distributions, can be found in the corresponding references provided in the table. Figure 3 compares the current predictions at the first three blade passing frequencies (BPFs) against the experiment and the predictions made by Kvurt and Stalnov. Again, the discrepancy between the predictions occur due to the different aerodynamic outputs from BEMT, but the tonal noise is predicted within a reasonable margin of error especially at out-of-plane observer locations. Unlike the previous steady frequency-domain methods, the KS model accurately predicts tonal noise even at and near the rotor rotating axis.

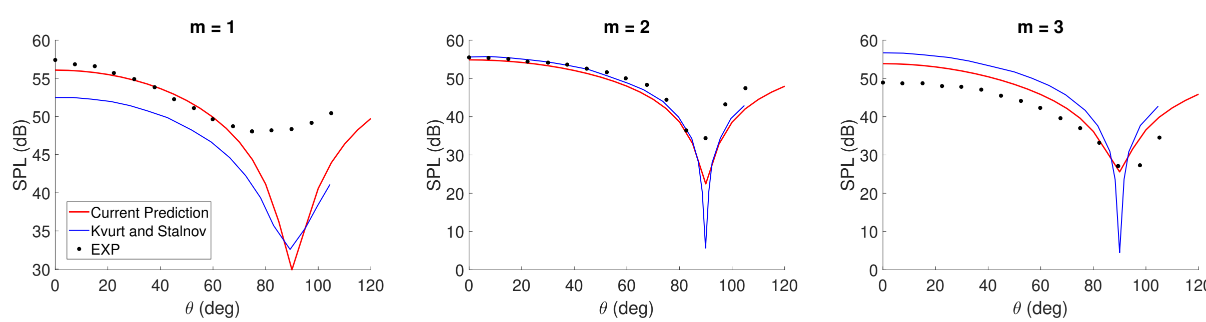

(a) (b) (c)

Fig. 3 Comparison of the tonal noise predictions of the Mejzlik Heavy Duty rotor with the experimental data [29] measured at 1.5 m (4.92 feet) away from the propeller hub and predictions made by Kvurt and Stalnov [29]: (a) $m = 1$, (b) $m = 2$, and (c) $m = 3$.

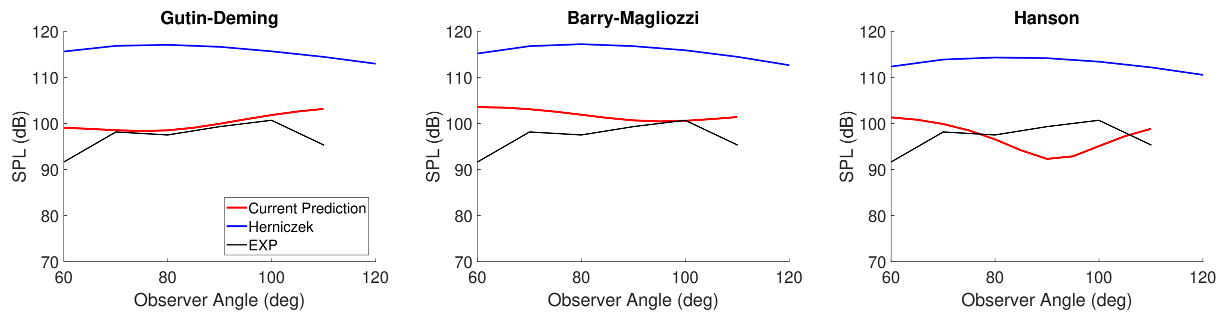

(a) (b) (c)

Fig. 4 Comparison of the first BPF tonal noise predictions of the SR-3 rotor with the experimental data [34] measured at 3.176 m (10.42 feet) away from the propeller hub and predictions made by Herniczek et al. [28, 30]: (a) Gutin-Deming, (b) Barry-Magliozzi, and (c) Hanson.

Since the BM and H models are also capable of predicting tonal noise for axial forward flight in addition to hover, the models are further verified using SR-3 propeller specified in Table 1. Although the GD model is only applicable for hover flight, the model is included in Fig. 4 to compare with the Herniczek et al.'s predictions. The KS model is also not valid for axial forward flight, so no separate verification of this model is conducted for axial forward flight. Figure 4 shows comparisons of the tonal noise at the first blade passing frequency (BPF) between the measurement data and our predictions as well as those made by Herniczek et al [28, 30]. for all models. Our predictions match more closely with the measurement data than the predictions made by Hericzek et al [28, 30]. Again, this discrepancy might be due to different aerodynamic inputs. Although the formulation by Gutin and Deming was derived for a hover condition, it surprisingly matches well with the case at an axial flight condition in this case. This observation agrees with Herniczek et al.'s results [28, 30]. Despite some discrepancies due to the limitations of the tonal noise prediction models, it is shown that the models can predict tonal noise of propellers at a wide range of observer angles under different flight conditions.

The broadband noise prediction models are not separately verified in the current paper since these models are empirically derived from experiments. These models will directly be applied in small rotor applications in the subsequent section to observe the capabilities of these models for small-scale rotors.

Validations for Small-Scale Rotors

Ideally twisted, APC, and DJI rotors are selected to study applicability of the steady frequency-domain tonal and broadband noise models on small rotors at multiple rotational speeds and rotor sizes, and W(B)STD8 rotors are selected to study the applicability of the unsteady frequency-domain tonal noise model. The naming convention of the W(B)STD8 rotors is as follows: B indicates a number of blades, 'STD' indicates standard rectangular blade shape, and the number at the end indicates the blade tip pitch. Therefore, the solidity increases as the number of blade (B) increases. Table 2 summarizes all rotor cases with their corresponding geometries and operating conditions. Detailed spanwise chord, thickness, and pitch distributions can be found from the references [33, 35–37]. The APC – Tinney and W(B)STD8 rotors have matrices of the thrust coefficients for the corresponding operating conditions. For instance, the experiments on the APC –Tinney rotors are conducted at every rotor radius and at every RPM, thus producing a 5×9 matrix of thrust coefficients. Likewise, the experiments on the W(B)STD8 rotors are conducted at every rotor solidity and at every RPM (3×3 matrix). The exact values of the thrust coefficients can be obtained from the corresponding references in the table. The microphone locations of all rotor cases are summarized in Tables 3 and 4. x is a coordinate along the rotor axis, and y and z are coordinates on the rotor plane. θ_0 indicates an elevation angle, negative being below the rotor plane and positive being above. The observer locations used on the APC rotor by Tinney [37] varies by the rotor diameter, and Table 4 shows the locations of the microphones where the tonal noise of these APC rotors were measured. Microphone 1 is located 9.5° above the rotor plane, and microphone 8 is located 45° below the rotor plane. Note that the x and z locations of the APC rotors by Tinney [37] are switched, compared to the original reference, to match with the coordinate system that is used in the current tonal noise models in this paper.

Table 2 Geometries and flight conditions for small rotor validations.

Rotors	Blade Number	Radius (m)	RPM	C_T	σ
Ideally Twisted [35]	4	0.1588	[3000, 5500]	[0.0112, 0.0137]	0.2550
APC – Zawodny [36]	2	0.14	[3600, 4200, 4800]	[0.0136, 0.0140, 0.0148]	0.1273
APC – Tinney [37]	2	[0.1016, 0.1270, 0.1524, 0.1778, 0.2032]	[1800:900:9000]	Matrix	0.0892
DJI [36]	2	0.12	[4800, 5400, 6000]	[0.0086, 0.0082, 0.0088]	0.0796
W(B)STD8 [33]	[2, 3, 4]	0.6095	[1070, 1605, 2150]	Matrix	[0.080, 0.119, 0.159]

Table 3 Observer locations for small rotor validations.

Rotors	x (m)	y (m)	z (m)	θ_0 (°)
Ideally Twisted [35]	-1.3020	0	1.8595	-35
APC – Zawodny [36]	-1.3470	0	1.3470	-45
APC – Tinney [37]		Variable		
DJI [36]	-1.3470	0	1.3470	-45
W(B)STD8 [33]	3.6576	0	0	90

Tonal Noise

The fundamental BPF tonal noise predictions of the ideally twisted rotor with rough surfaces at 3000 RPM and 5500 RPM are shown in Figs. 5(a) and 5(b), respectively. All models poorly predict the noise at a lower RPM of 3000 RPM. However, at a higher RPM, Gutin and Deming (GD) and Barry and Magliozzi (BM) formulations predict the first BPF tonal noise accurately. Hanson (H) formulation consistently shows a significant under-prediction for ideally twisted rotors.

A better performance of the tonal noise models is observed for APC rotors. Figures 6(a) through 6(c) show the first two BPFs tonal noise predictions of the APC rotors at 3600 RPM, 4200 RPM, and 4800 RPM, respectively. All models over-predict the fundamental BPF tonal noise by at least 5.27 dB at 3600 RPM, 4.27 dB at 4200 RPM, and 5.14 dB at 4800 RPM. However, they under-predict second BPF tonal noise by at least 9.05 dB at 3600 RPM, 3.54 dB at 4200 RPM, and 0.14 dB at 4800 RPM. The second BPF tonal noise prediction improves with increasing RPM, while the margin of an error for the first BPF tonal nosie prediction is fairly consistent. The models capture the trend of increasing noise peak magnitudes with increasing RPM. The noise prediction by BM formulation is the highest among the three formulations at all rotational speeds and BPFs. The tonal noise prediction models seem to perform well for some cases but not for all small rotor cases.

A more intensive set of experiments involving APC rotors [37] is used to further study the performance of the current tonal noise prediction models. Figures 7 and 8 show the tonal noise prediction performance of the three steady frequency-domain models with varying rotational speed and rotor diameter at two different observer locations. The rotational speed in RPM is increased from 1800 to 9000 with an increment of 900 RPM, except for the rotor with $D = 16$ in, for which the rotational speed is limited to a maximum of 7200 RPM. The diameter of the rotor is varied from 8 to 16 in, with an increment of 2 in. At the microphone 1 location in Fig. 7, the tonal noise predictions are in good agreement with the measurement at all RPMs except at the lowest RPM. The BM model consistently predicts SPL to be higher than the other two models, while the GD and H models are fairly similar up to $D = 12$ in. For higher diameters, the H model provides the best agreement with the experimental data. At the microphone 8 location in Fig. 8, all models over-predict tonal noise at all RPM, but the over-prediction is especially magnified at higher RPM. The BM model remains to predict tonal noise higher than the other two models. The GD and H models give almost the same

Table 4 Microphone locations used in the experiment by Tinney [37].

Microphone	x (m)	y (m)	z (m)	θ_0 (°)
1	0.5D	0	3D	9.5
8	-3.0D	0	3D	-45

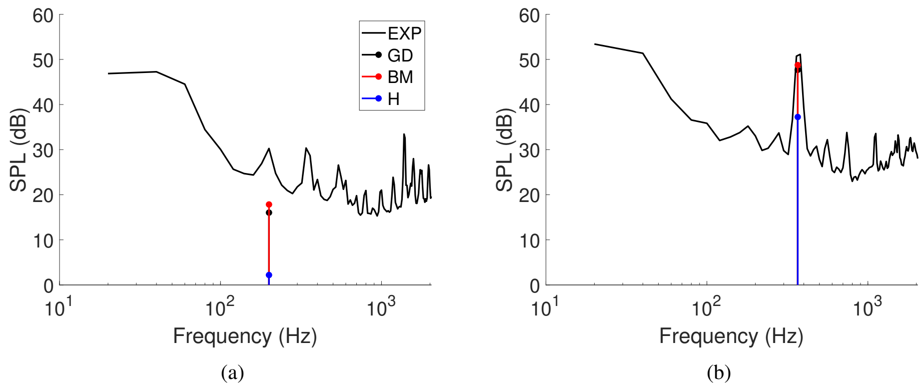

(a) (b)

Fig. 5 First BPF tonal noise predictions of an ideally twisted rotor at (a) 3000 RPM and (b) 5500 RPM.

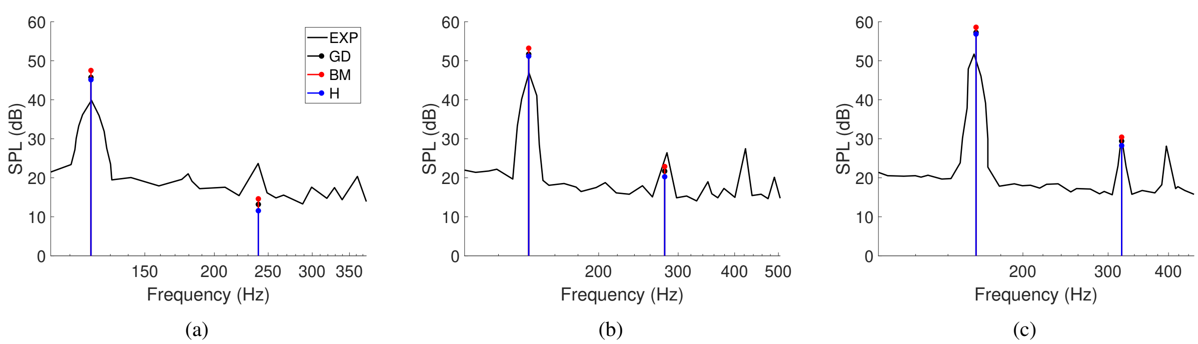

(a) (b) (c)

Fig. 6 First two BPF tonal noise predictions of the APC rotor at (a) 3600 RPM, (b) 4200 RPM, and (c) 4800 RPM.

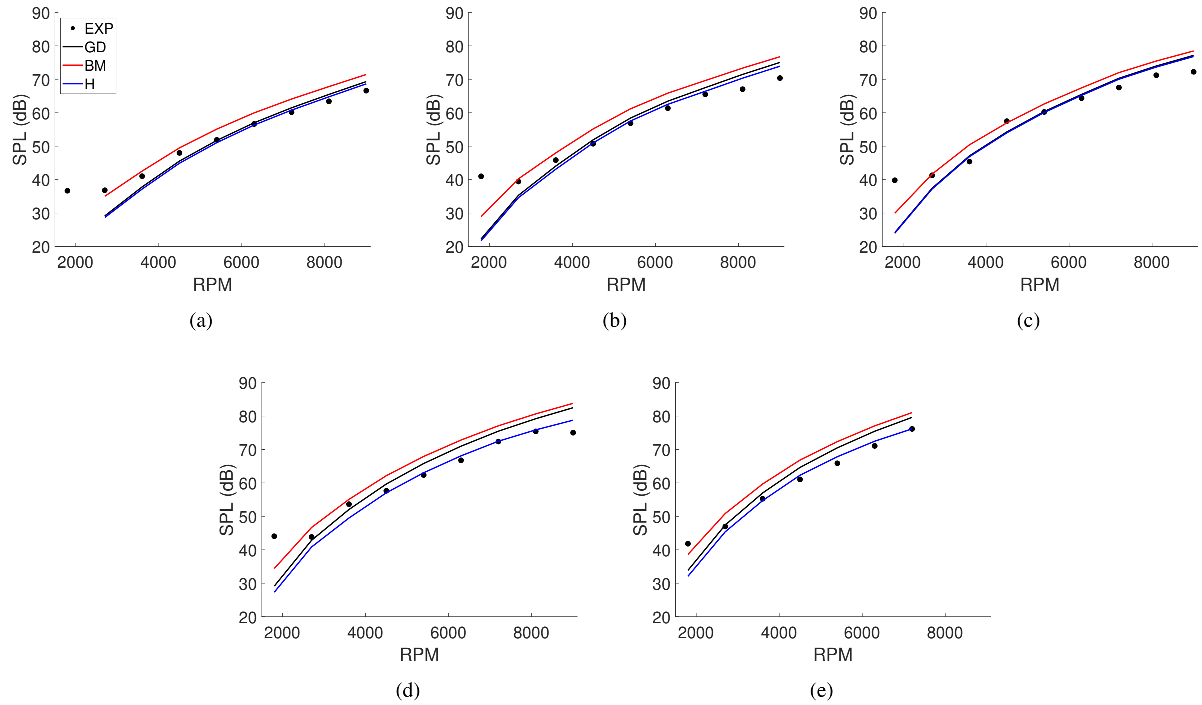

Fig. 7 Comparisons of the fundamental BPF tonal noise between the measurements [37] and predictions on APC rotors with varying rotor diameters at microphone location 1: (a) $D = 8$ **in (0.2032 m), (b)** $D = 10$ **in (0.2540 m), (c)** $D = 12$ **in (0.3048 m), (d)** $D = 14$ **in (0.3556 m), and (e)** $D = 16$ **in (0.4064 m).**

results for all diameters. Figures 7 and 8 demonstrate that the steady frequency-domain models perform well near the rotor plane, but the prediction accuracy diminishes as an observer moves farther away from the rotor plane. Despite some over-predictions, all models correctly capture the trend that SPL increases with RPM.

The steady frequency-domain models are also validated against the DJI rotor [36] with three different rotational speeds. As shown in Fig. 9, the BM model predicts SPL higher than the other two models at all BPFs and RPMs, while the predictions by the GD and H models remain similar in magnitude with the GD model predicting slightly greater than the H model. The fundamental BPF tonal noise is over-predicted by at least 2.42 dB at 4800 RPM, 2.63 dB at 5400 RPM, and 3.93 dB at 6000 RPM. The performance of these models are better with the DJI rotor cases than the Zawodny's APC rotor cases [36] that were shown in Fig. 6. Since the DJI rotor has a lower thrust coefficient at a relatively high RPM, the magnitude of the over-prediction is smaller than that of APC rotor cases. The second harmonic tonal noise is under-predicted by at least 7.43 dB at 4800 RPM and 5.12 dB at 5400 RPM but is over-predicted by at least 3.85 dB at 6000 RPM. There is no definitive trend in the performance of the models to predict the second harmonic tonal noise, but they capture the increasing noise trend with increasing the RPM.

In addition to the steady models, an unsteady model is validated against the available data. Since the steady frequency-domain models cannot capture noise along the rotor rotating axis, the main interest of the validation of the unsteady model is its capability to predict noise directly above or below a rotor plane. Due to a lack of measurement data of the drone rotors along the rotor axis, small-scale propellers [33] are used to validate noise predictions along the rotor axis. However, the work of Kvurt and Stalnov [29] already shows the validity of this unsteady model on a small rotor, so the validation of this model on the small-scale propeller extends the validity of the unsteady frequency-domain model to a wider range of rotors. Figure 10 shows the fundamental BPF tonal noise of the three rotors with different rotor solidity, each of which is tested at three different rotational speeds. All of these predictions and measurements are obtained from the observer location 3.6576 m directly above the rotor hub. The unsteady model performs the best in the two-bladed rotor case in Fig. 10(a) since the largest difference between the prediction and the measurement is 3.29 dB at 1070 RPM. At a relatively high RPM, the model's predictions also agrees with the measurement in the two-bladed rotor case. As the number of blades increases, a significant over-prediction at high RPM is observed. For the three-bladed

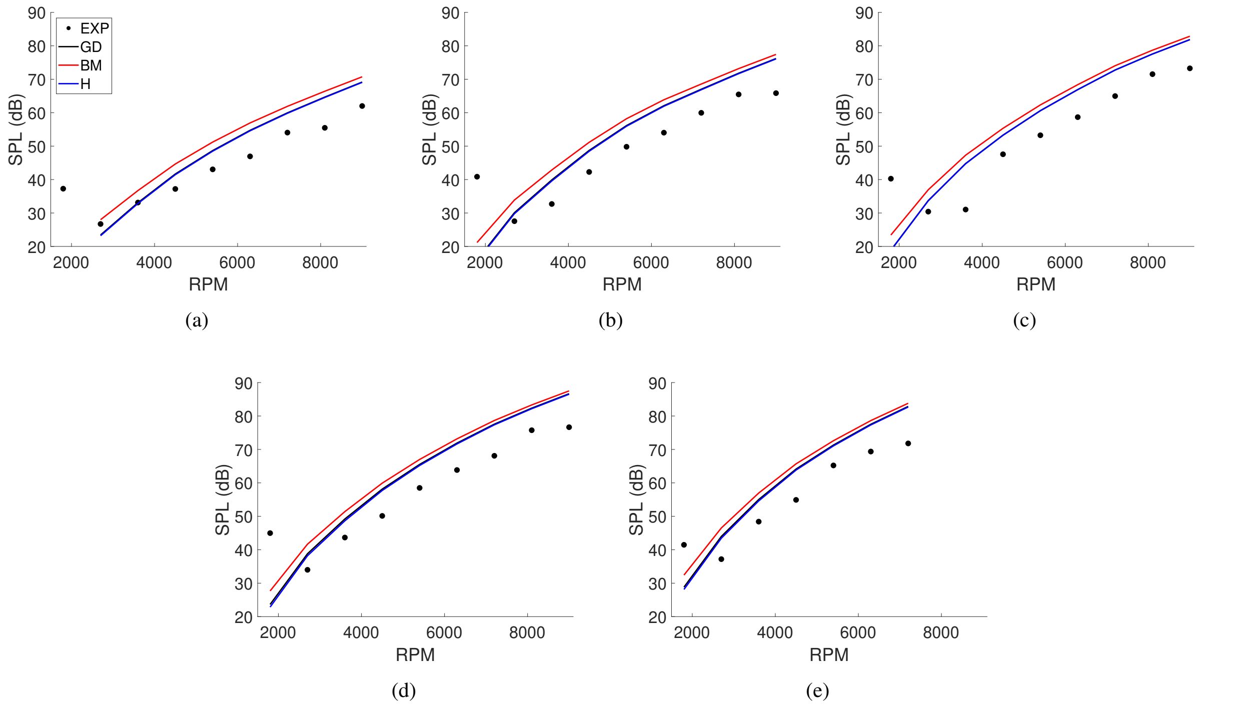

Fig. 8 Comparisons of the fundamental BPF tonal noise between the measurements [37] and predictions on APC rotors with varying rotor diameters at microphone location 8: (a) $D = 8$ in (0.2032 m), (b) $D = 10$ in (0.2540 m), (c) $D = 12$ in (0.3048 m), (d) $D = 14$ in (0.3556 m), and (e) $D = 16$ in (0.4064 m).

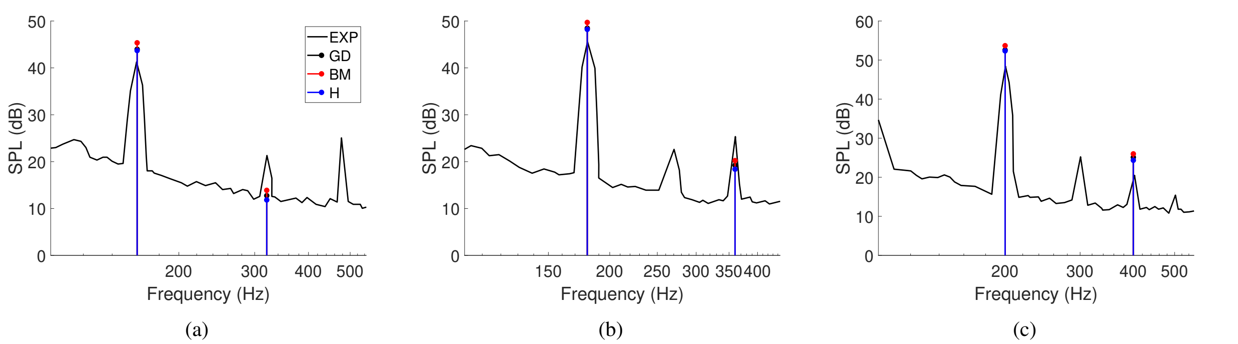

Fig. 9 First two BPF tonal noise predictions of the DJI rotor at (a) 4800 RPM, (b) 5400 RPM, and (c) 6000 RPM.

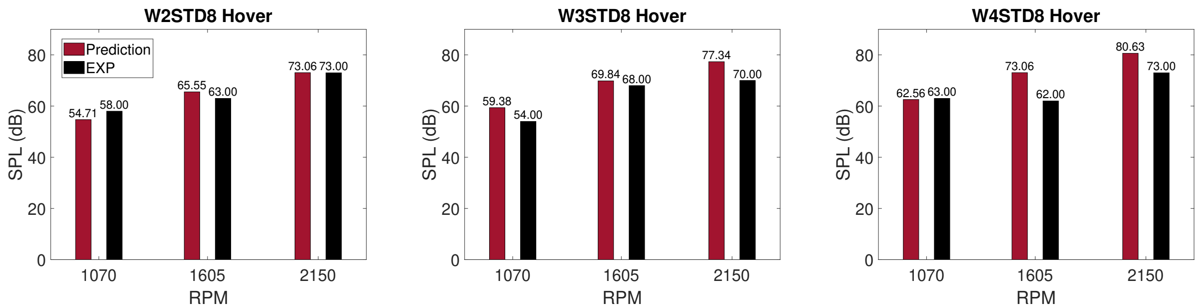

(a) (b) (c)

Fig. 10 Comparison of the fundamental BPF tonal noise at 3.6576 m directly above a rotor hub: (a) W2STD8, (b) W3STD8, and (c) W4STD8.

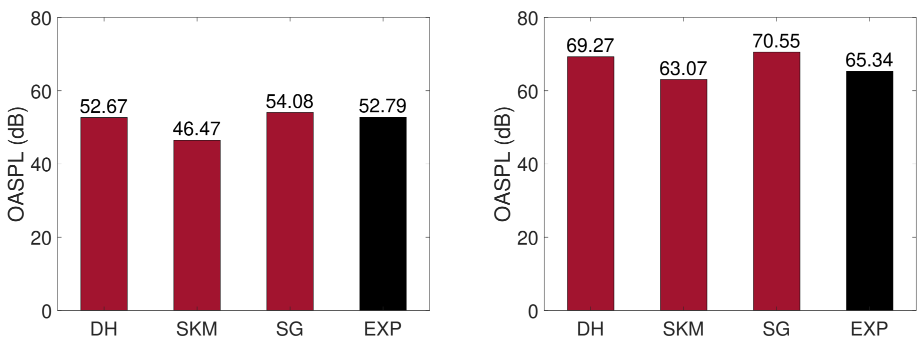

(a) (b)

Fig. 11 Broadband noise predictions of an ideally twisted rotor at (a) 3000 RPM and (b) 5500 RPM.

rotor case, the model over-predicts the tonal noise by 7.34 dB at 2150 RPM. The tonal noise prediction is even larger by 11.06 dB than the measurement at 1605 RPM for the four-bladed rotor case. The highest RPM case corresponds to a tip Mach of 0.4, and the lowest RPM case corresponds to a tip Mach of 0.2. At a higher blade tip speed, the model is expected to over-predict the tonal noise, but the model's prediction performance improves at a lower blade tip speed.

Broadband Noise

Applicability of the empirical broadband noise models is studied in addition to the tonal noise in this subsection. Figures 11(a) and 11(b) compare the predicted overall sound pressure levels (OASPLs) of broadband noise produced from the ideally twisted rotor at 3000 RPM and 5500 RPM, respectively, with the experimental data [35]. At 3000 RPM, the prediction by DH model matches very well with the experiment. SG model over-predicts OASPL by 1.82 dB, while SKM model under-predicts by 5.65 dB. At 5500 RPM, DH and SG models over-predict OASPL by 4.05 dB and 5.34 dB, respectively, while SKM model under-predicts by 2.15 dB. Considering that the models only take the blade tip velocity and blade loading (C_T/σ) as the main inputs, the models predict OASPLs with a reasonable margin of error. The models can also capture the trend of increasing OASPL with increasing RPM.

APC rotor cases have higher blade loading than the ideally twisted rotor cases. Table 2 shows that the APC rotor has a lower rotor solidity but higher thrust coefficients than the ideally twisted rotor at similar RPMs. Figures 12(a) through 12(c) show OASPL of broadband noise produced from the APC rotors at 3600 RPM, 4200 RPM, and 4800 RPM, respectively. Since the models predict OASPL based on the blade loading and blade tip velocity, the APC rotor with the higher blade loading shows higher noise levels than the ideally twisted rotor. At 3600 RPM, SKM model matches very well with the experiment, while DH and SG models over-predict OASPL by 6.72 dB and 6.82 dB, respectively. At 4200 RPM, all models over-predict OASPL by 10.54 dB (DH), 4.34 dB (SKM), and 10.6 dB (SG), respectively.

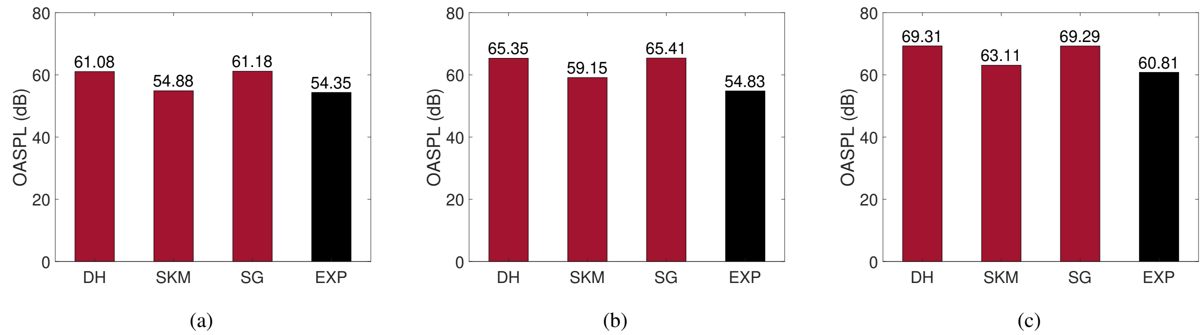

Fig. 12 Overall sound pressure level predictions of broadband noise from the APC rotor at (a) 3600 RPM, (b) 4200 RPM, and (c) 4800 RPM.

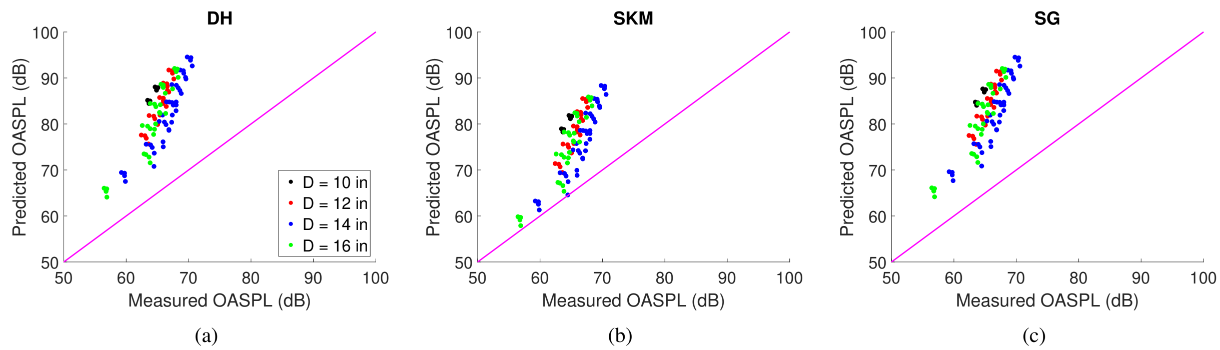

Fig. 13 Comparison between the measured OASPL and the predictions of broadband noise for the APC - Tinney rotor by (a) DH model, (b) SKM model, and (c) SG model.

The difference between the measurement and the predictions is especially large at 4200 RPM since the models expect the noise to increase with increasing RPM, but in the experimental data, OASPL does not increase noticeably. Since these models can only compute OASPL without individual sources, it is difficult for the models to reveal what causes the experiment OASPL to remain similar between 3600 and 4200 RPMs and respond accordingly. At 4800 RPM, all models over-predict OASPL by 8.52 dB (DH), 2.32 dB (SKM), and 8.49 dB (SG), respectively. SKM model consistently predicts OASPLs within ±5 dB margin of error, while the other two models show larger prediction errors.

Using the experiment data [37] of the APC - Tinney rotors with varying rotor diameter and RPM, the OASPL of broadband is obtained and compared with the predictions made by the DH, SKM, and SG models in Fig. 13. The y-axis is the predicted OASPL by the corresponding model, and the x-axis is the experimentally obtained OASPL of the APC rotor. A total of 99 test cases are used in Fig. 13 at various diameters, RPMs, and observer locations. Some cases with the low RPM or small diameter from the original reference are omitted in the figure since they exhibited signs of laminar boundary layer vortex shedding (LBLVS) noise and the empirical broadband noise models are not designed to capture LBLVS noise. LBLVS noise is expected to occur at low RPM due to the lower local Reynolds numbers on the blade [35]. The data closer to the diagonal line in Fig. 13 indicate the match of the prediction model with the experiment data. However, all models show significant over-predictions of broadband OASPL, which is consistent with the performance of the models shown in Fig. 12. Among the three models, the SKM model shows the least over-predictions, and some rotors with D = 14 in and D = 16 in at lower RPMs agree with the measured OASPL.

Unlike the ideally twisted and APC rotors, the DJI rotor has significantly lower thrust coefficients for its relatively high RPMs. The OASPL predictions by the three models are shown in Fig. 14. For the rotor with a relatively lower thrust coefficient, the noise predictions by the DH and SG models match well with the experiment data at 4800 RPM in Fig. 14(a), but the SKM model significantly under-predicts the OASPL. As the RPM increases, the predicted OASPL magnitude from all models increase, while the experiment data remain relatively unchanged. Although the experimental

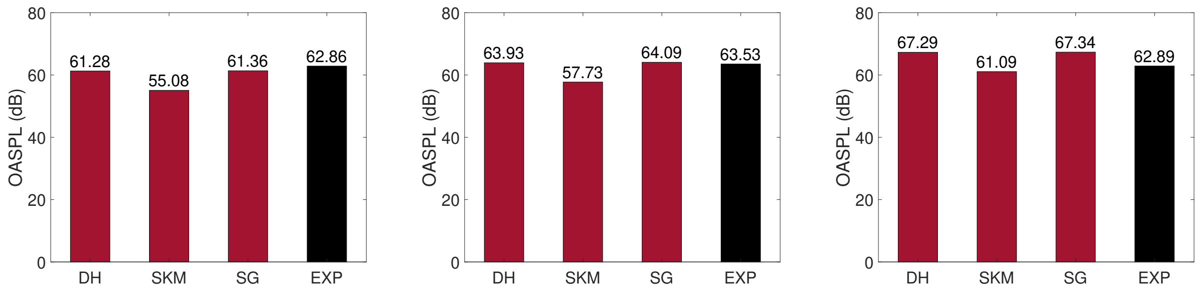

(a) (b) (c)

Fig. 14 Overall sound pressure level predictions of broadband noise from the DJI rotor at (a) 4800 RPM, (b) 5400 RPM, and (c) 6000 RPM.

OASPL is relatively constant, the broadband noise spectrum may still show an increase in the noise levels at a certain frequency range with increasing RPM. Since the OASPL is the summation of the noise levels over the entire frequency range, a decrease in the noise level at other frequency ranges may counteract the increase in the noise level with the RPM increase. However, empirical models are not capable of correlating the detailed flow physics that could have contributed to the actual noise results, and they are only limited to the input design variables, which causes the predicted OASPL to increase with increasing the RPM.

From the presented rotor cases for the broadband noise predictions, the DH and SG models show similar magnitudes in the OASPL predictions, while SKM model always predicts at least 6 dB lower than the other two models. Overall, SKM model provides the closest results to the experimental data. Comparing the noise predictions by DH and SG models shows that the difference in the value of the exponent on the blade loading term in Eqs. (27) and (29) does not significantly affect the OASPL predictions. However, comparing the noise predictions by SKM model with the other two models shows that the constant correction term that is subtracted at the end of each model (Eqs. (27), (28), and (29)) significantly alters the values of the OASPL predictions. This constant correction term may need to be modified to be a function of rotor performance variables to minimize over-prediction under a high blade loading condition and prevent under-prediction at a low blade loading condition.

Conclusion

With the rising interest in the eVTOL and drone industries, efficient methods for predicting noise from small rotors are needed. However, the existing tonal and broadband noise prediction methods presented in this paper that were developed based on a large rotor, such as a propeller and a helicopter rotor, may have limited success for small rotor noise predictions. The applicability of these models were investigated, and their capabilities and limitations on smaller rotors were analyzed. Verifications and validations against available experimental small-scale propeller and drone noise data showed that the tonal noise predictions by the BM model were consistently higher than the two other steady frequency-domain models (GD and H). All models tended to over-predict the fundamental BPF tonal noise, and the magnitude of the over-predictions was amplified as an observer moves farther away from the rotor plane. A notable limitation of these steady frequency-domain models was that the loading noise cannot be captured along the rotor axis. In order to improve this limitation, an unsteady frequency-domain model (KS) was investigated. Despite some over-predictions at higher blade tip speeds, the model sufficiently predicted the tonal noise along the rotor axis, providing a more complete directivity analysis.

Furthermore, empirical broadband noise OASPL models were investigated to understand their limitations and performance on the small rotors. The DH and SG models showed consistent over-predictions by similar magnitude in all small rotor cases except the DJI rotor cases which had a relatively smaller thrust coefficient. The OASPL predictions by the SKM model were noticeably smaller than the predictions by the other two models, thus accurately predicting the OASPL for some cases. However, a statistical analysis on the APC rotor showed that a large amount of data were still over-predicted. Although the SKM model showed the best performance among the three empirical broadband noise OASPL models that were analyzed in this paper, none of these models were robust when applied to small rotors. Since the noise predictions were found to be more sensitive to the constant at the end of each model's expression

(Eqs. (27), (28), and (29)), this constant may be further modified as a function of rotor design input parameters to improve the noise prediction capability for small rotors.

Acknowledgements

A funding for this study was provided by NASA's University Leadership Initiative (ULI) project.

References

[1] Johnson, W., *Noise*, Cambridge Aerospace Series, Cambridge University Press, 2013, p. 493–544. https://doi.org/10.1017/CBO9781139235655.015.

[2] Ffowcs Williams, J. E., and Hawkings, D. L., "Sound Generated by Turbulence and Surfaces in Arbitrary Motion," *Philosophical Transactions of the Royal Society*, Vol. A264, No. 1151, 1969, pp. 321–342.

[3] Brooks, T. F., Pope, D. S., and Marcolini, M. A., "Aifoil Self-Noise and Prediction," NASA RP 1218, 1989.

[4] Lee, S., Ayton, L., Bertagnolio, F., Moreau, S., Chong, T. P., and Joseph, P., "Turbulent Boundary Layer Trailing-Edge Noise: Theory, Computation, Experiment, and Application," *Progress in Aerospace Sciences*, Vol. 126, October, 2021, p. 100737. https://doi.org/10.1016/j.paerosci.2021.100737.

[5] Farassat, F., "Derivation of Formulations 1 and 1A of Farassat," Tech. Rep. NASA/TM-2007–214853, NASA Langley Research Center, 2007.

[6] Jia, Z., and Lee, S., "Computational Study on Noise of Urban Air Mobility Quadrotor Aircraft," *Journal of American Helicopter Society*, Vol. 67, No. 1, January, 2022, pp. 1–15. https://doi.org/10.4050/JAHS.67.012009.

[7] Jia, Z., and Lee, S., "High-Fidelity Computational Analysis on the Noise of a Side-by-Side Hybrid VTOL Aircraft," *Journal of American Helicopter Society*, Vol. 67, No. 2, April, 2022, pp. 1–14. https://doi.org/10.4050/JAHS.67.022005.

[8] Sagaga, J., and Lee, S., "Acoustic Predictions for the Side-by-Side Air Taxi Rotor in Hover," 77^{th} VFS International Annual Forum, Virtual Event, May 10–14, 2021.

[9] Guttin, L., "On the Sound Field of a rotating Propeller," Tech. Rep. NACA–TM–1195, National Advisory Committee for Aeronautics, 1936.

[10] Deming, A. F., "Noise from Propellers with Symmetrical Sections at Zero Blade Angle," Tech. Rep. NACA–TN–605, National Advisory Committee for Aeronautics, July 1937.

[11] Barry, F. W., and Magliozzi, B., "Noise Detectability Prediction Method for Low Tip Speed Propellers," Tech. Rep. AFAPL–TR–71–37, Air Force Aero Propulsion Laboratory, June 1971.

[12] Hanson, D. B., "Influence of Propeller Design Parameters on Far-Field Harmonic Noise in Forward Flight," *AIAA Journal*, Vol. 18, No. 11, November, 1980, pp. 1313–1319. https://doi.org/10.2514/3.50887.

[13] Hanson, D. B., "Helicoidal Surface Theory for Harmonic Noise of Propellers in the Far Field," *AIAA Journal*, Vol. 18, No. 10, October, 1980, pp. 1213–1220. https://doi.org/10.2514/3.50873.

[14] Li, S., and Lee, S., "Prediction of Rotorcraft Broadband Trailing-Edge Noise and Parameter Sensitivity Study," *Journal of the American Helicopter Society*, Vol. 65, No. 4, October, 2020, pp. 1–14. https://doi.org/10.4050/JAHS.65.042006.

[15] Li, S., and Lee, S., "Prediction of Urban Air Mobility Multi-Rotor VTOL Broadband Noise Using UCD-QuietFly," *Journal of the American Helicopter Society*, Vol. 66, February, 2021, p. 032004. https://doi.org/10.4050/JAHS.66.032004.

[16] Li, S., and Lee, S., "Acoustic Analysis and Annoyance Assessment of a Quiet Helicopter for Air Taxi Operations," *Journal of American Helicopter Society*, March, 2022. https://doi.org/10.4050/JAHS.67.032001.

[17] Amiet, R. K., "Acoustic radiation from an airfoil in a turbulent stream," *Journal of Sound and Vibration*, Vol. 41, 1975, pp. 407–420.

[18] Roger, M., and Moreau, S., "Back-Scattering Correction and Further Extensions of Amiet's Trailing Edge Noise Model. Part 1: Theory," *Journal of Sound and Vibration*, Vol. 286, 2005, pp. 477–506.

[19] Roger, M., and Moreau, S., "Extensions and Limitations of Analytical Airfoil Broadband Noise Models," *International Journal of Aeroacoustics*, Vol. 9, No. 3, May, 2010, pp. 273–305. https://doi.org/10.1260/1475-472X.9.3.273.

[20] Li, S., and Lee, S., "Predictions and Validations of Small-Scale Rotor Noise Using UCD-QuietFly," Proceedings of the American Helicopter Society Technical Conference on Aeromechanics Design for Transformative Vertical Flight, San Jose, CA, January 25–27, 2022.

[21] Lee, S., "Empirical Wall-Pressure Spectral Modeling for Zero and Adverse Pressure Gradient Flows," *AIAA Journal*, Vol. 56, No. 5, May, 2018, pp. 1818–1829. https://doi.org/10.2514/1.J056528.

[22] Lee, S., and Shum, J. G., "Prediction of Airfoil Trailing Edge Noise Using Empirical Wall Pressure Spectrum Models," *AIAA Journal*, Vol. 57, No. 3, March, 2019, pp. 888–897. https://doi.org/10.2514/1.J057787.

[23] Yudin, E. Y., "On the Vortex Sound from Rotating Rods," Tech. Rep. NACA–TM–1136, National Advisory Committee for Aeronautics, March 1947.

[24] Davidson, I. M., and Hargest, T. J., "Helicopter Noise," *Journal of the Royal Aeronautical Society*, Vol. 69, May, 1965, pp. 325–336. https://doi.org/10.1017/s0001924000059583.

[25] Schlegel, R., King, R., and Mull, H., "Helicopter Rotor Noise Generation and Propagation," Tech. Rep. USAAVLABS–TR–66–4, U.S. Army Aviation Materiel Laboratories, October 1966.

[26] Stuckey, T. J., and Goddard, J. O., "Investigation and Prediction of Helicopter Rotor Noise Part 1. Wessex Whirl Tower Results," *Journal of Sound Vibration*, Vol. 5, No. 1, January, 1967, pp. 50–80. https://doi.org/10.1016/0022-460X(67)90178-2.

[27] Pegg, R. J., "A Summary and Evaluation of Semi-Empirical Methods for the Prediction of Helicopter Rotor Noise," Tech. Rep. NASA–TM–80200, NASA, December 1979.

[28] Herniczek, M. T., Feszty, D., Meslioui, S., and Park, J., "Applicability of Early Acoustic Theory for Modern Propeller Design," AIAA AVIATION Forum, Denver, Colorado, June 5–9, 2017.

[29] Kvurt, A., and Stalnov, O., "From the Blade Geometry to Prediction of Tonal Noise Component in Hover," 28^{th} AIAA/CEAS Aeroacoustics 2022 Conference, Southampton, UK, June 14–17, 2022.

[30] Herniczek, M. T. K., Feszty, D., Meslioui, S., Park, J., and Nitzsche, F., "Evaluation of Acoustic Frequency Methods for the Prediction of Propeller Noise," *AIAA Journal*, Vol. 57, No. 6, June, 2019, pp. 2465–2478. https://doi.org/10.2514/1.J056658.

[31] Garrick, I. E., and Watkins, C. E., "A Theoretical Study of the Effect of Forward Speed on the Free-Space Sound-Pressure Field Around Propellers," Tech. Rep. NACA–TM–79844, National Advisory Committee for Aeronautics, 1954.

[32] Johnson, W., *Rotorcraft Aeromechanics*, Cambridge University Press, 32 Avenue of the Americas, New York, NY 10013-2473, USA, 2013, Chap. 10, pp. 366–413.

[33] Brown, D., and Ollerhead, J. B., "Propeller Noise at Low Tip Speeds," Tech. Rep. AFAPL–TR–71–55, Air Force Aero Propulsion Laboratory, September 1971.

[34] Brooks, B. M., and Metzger, F. B., "Acoustic Test and Analysis of Three Advanced Turboprop Models," Tech. Rep. NASA–CR–159667, National Aeronautics and Space Administration, January 1980.

[35] Pettingill, N. A., Zawodny, N. S., Thurman, C. S., and Lopes, L. V., "Acoustic and Performance Characteristics of an Ideally Twisted Rotor in Hover," AIAA Scitech 2021 Forum, Virtual Event, January 19–21, 2021.

[36] Zawodny, N. S., Boyd, D. D., and Burley, C. L., "Acoustic Characterization and Prediction of Representative, Small-Scale Rotary-Wing Unmanned Aircraft System Components," American Helicopter Society Annual Forum, West Palm Beach, FL, May 17, 2016.

[37] Tinney, C., and Valdez, J., "Acoustic Scaling for Small Rotors in Hover," AHS International 75^{th} Annual Forum and Technology Display, Philadelphia, Pennsylvania, May 14–15, 2019.